Applied Catalysis B: Environmental 156–157 (2014) 249–256

Contents lists available at ScienceDirect

Applied Catalysis B: Environmental

journal homepage: www.elsevier.com/locate/apcatb

New insight into photoelectric converting CO_2 to CH_3OH on the one-dimensional ribbon CoPc enhanced Fe_2O_3 NTs

Zhongxue Yang, Jinfeng Xu[1], Chenxiao Wu, Hua Jing, Peiqiang Li*, Hongzong Yin*

College of Chemistry and Material Science, Shandong Agricultural University, 271018, PR China

ARTICLE INFO

Article history:
Received 24 December 2013
Received in revised form 2 March 2014
Accepted 9 March 2014
Available online 18 March 2014

Keywords:
Fe_2O_3 NTs
Cobalt phthalocyanine
Photoelectrocatalytic reduction
Carbon dioxide

ABSTRACT

The Fe_2O_3 NTs was in situ prepared by the anodic oxidation method. One-dimensional ribbon cobalt phthalocyanine (CoPc-Rs) was loaded onto Fe_2O_3 NTs. The morphology structure analysis showed that the CoPc-Rs with length of 7.1 μm and width of 700 nm distributed on the Fe_2O_3 NTs surface evenly and it tended to grow toward (0 0 1) crystal plane. After assembling CoPc-Rs onto Fe_2O_3 NTs, on the one hand, the photocatalytic performance was enhanced due to the improvement of absorbing visible light and the relative narrower energy band gap. On the other hand, electrocatalytic ability was improved by the resistance value reduces (900 Ω) and the overpotential drops (40 mV). In the photoelectrocatalytic reduction process at −1.3 V, the net current density ($i_{CO2} - i_{N2}$) of CoPc-Rs/Fe_2O_3 NTs was 7.65 times that of the Fe_2O_3 NTs. The overpotential of photoelectrocatalytic reduction of CO_2 on CoPc-Rs/Fe_2O_3 NTs brought forward 100 mV than that of Fe_2O_3 NTs, which indicated that the CoPc-Rs/Fe_2O_3 NTs exerted outstanding photoelectrocatalytic reduction performance. The methanol concentration of photoelectrocatalytic reduction of CO_2 was 138 μmol L^{-1} cm^{-2}, it was greater than the simple addition (126 μmol L^{-1} cm^{-2}) of photocatalysis and electrocatalysis, which embodied the excellent synergistic effect of photocatalytic reduction and electrocatalytic reduction. The faradaic current efficiency reached up to 84.6% at present.

1. Introduction

Environment pollution and energy crisis are serious influencing factors for human sustainable development. Now, the vast CO_2 have been released by burning fossil fuel, which given rise to turning climate awfully and elevating sea horizon, and other seriously environmental problems. With the increasing attention for environment pollution and resource shortage, how to reduce the content of CO_2 in the atmosphere, effectively utilize the CO_2, and build the environmentally friendly and non-fossil fuel of the new renewable energy system have been treated as the most popular research hotspots and aroused attention in the world. Under some certain conditions, transforming CO_2 into useful resources not only decreased the discharge of CO_2, but also achieved the resources recycling. Now, this research field including the high temperature heterogeneous and homogeneous catalytic hydrogenation, the electrocatalytic (EC) reduction and photocatalytic (PC) reduction, and so on [1–7].

CO_2 is also a very precious C1 resource, the techniques about converting CO_2 to alcohols, etc. chemicals have been reported. The key problem is the origin of hydrogen, the hydrogen in the traditional conversion methods still comes from fossil resources, so the practical significance of entire process is not obvious [8,9]. However, the hydrogen resources of PC reduction CO_2 and EC reduction CO_2 come from water, and this way is a clean, environment friendly and new renewable energy method, so it is an excellent advanced technology on catalytic reduction of CO_2 [10–15].

TiO_2 is one of the hottest researching material in the PC reductions, but its energy gap (E_g) is 3.2 eV, and it could be only excited by ultraviolet light under 385 nm, therefore, the visible light could not be used fully, which limited the application [16–18]. While the E_g of Fe_2O_3 is 2.20 eV, it could absorb visible light under 563 nm, and the cost is inexpensive, so Fe_2O_3 has caught more attention among the photocatalysts over the past decades [19]. One-dimensional grew Fe_2O_3 NTs nanostructure has better PC activity among many Fe_2O_3 nanostructures for its large specific surface area, high active sites and strong charge transportation ability [20]. From the aspect of energy band, the valence band of Fe_2O_3 is 1.92 eV, which has strong PC oxidation ability [21]. So Fe_2O_3 has been applied to PC oxidation degradation of organic pollution extensively. However, the

* Corresponding authors at: College of Chemistry and Material Science, Shandong Agricultural University, 61 Daizong Road, Tai'an, Shandong 271018, PR China. Tel.: +86 0538 8249017.
E-mail addresses: chem_carbon@outlook.com, pqli@sdau.edu.cn (P. Li).
[1] Co-first author.

http://dx.doi.org/10.1016/j.apcatb.2014.03.012
0926-3373/

conduction band of Fe_2O_3 is 0.28 eV, so it cannot be applied to those reactions needed more negative reduction potential.

To improve the upper disadvantages, the several method is grafting the material with negative conduction band. It can enhance the reduction ability by the energy band matched. There are usually two choices to graft materials. One is the inorganic material, and there are a lot studies about this aspect [22]. The other is organic light-sensitive material [23], but there is few study on PC reduction. Therefore, specific morphology of organic light-sensitive materials was assembled on Fe_2O_3 NTs to broad the visible light absorption and increase the PC reduction ability of Fe_2O_3 NTs.

Phthalocyanine (Pc) with 18 electronic flat structure and stable property is a potential functional material [24]. Cobalt phthalocyanine (CoPc) is a higher catalytic activity among the Pc compounds. So one-dimensional CoPc-Rs were assembled onto the Fe_2O_3 NTs to obtain CoPc-Rs/Fe_2O_3 NTs, the visible light absorption ability and PC reduction ability of Fe_2O_3 NTs were expected to be enhanced simultaneously.

Meanwhile, CoPc has outstanding electron transfer ability, it can greatly decrease the overpotential of EC and effectively improve the EC properties of catalyst. Consequently, the work of photoelectrocatalytic (PEC) reduction of CO_2 on CoPc-Rs/Fe_2O_3NTs was carried out. Based on the excellent PC reduction performance, it would be expected to realize the synergistic effect between PC and EC on the electrode at the same time. This research offered a new method for designing the catalyst for PEC synergistic reduction of CO_2, it also had positive significance for reducing carbon emission and cycling carbonaceous energy.

2. Experimental methods

Preparation of Fe_2O_3 NTs: iron sheet was mechanically polished, completely washed, and etched 10 min in 10 wt% oxalic acid. The iron sheet was used as anode and titanium sheet as cathode. The electrolyte was made up 0.25 wt% NH_4F (V_{glycol}:V_{water} = 97:3) solution. The anodization experiment was performed under 30 V for 2 h (20 °C). After sonicating for 5 min, the samples were put in a muffle furnace (KSL-1100X) under oxygen atmosphere with the flow rate of 60 sccm (standard cubic centimeters min^{-1}), then heated to 500 °C with rate of 3 °C min^{-1} and maintained at 500 °C for 2 h. Then it was cooled to room temperature with the rate of 3 °C min^{-1}. Therefore, Fe_2O_3 NTs were converted to crystalline structure from amorphous structure.

Preparation of CoPc-Rs/Fe_2O_3NTs: phthalic anhydride, carbamide, ammonium molybdate and cobalt chloride hexahydrate were mixed together by proportion agglomerated at 200 °C for 2 h in N_2 atmosphere to get CoPc compound. Then the compound was grinded to powder and rinsed by 4 mol L^{-1} HCl and 10 wt% NaOH, filtrated and stored under 100 °C, and then got a dark blue solid powder. CoPc, β-CD, DMF, H_2O were mixed together by proportion ($M_{\beta\text{-CD}}$:M_{CoPc} = 2:1, 10 mL DMF + 5 mL H_2O), then spun on Fe_2O_3NTs and finally CoPc-Rs/Fe_2O_3NTs was obtained.

The surface morphologies of the as-prepared samples were characterized by scanning electron microscopy (SEM, Philips XL30 FEG) with accelerated voltage of 20 kV. The crystalline structures were characterized by X-ray diffraction (XRD, Rigaku D/MAX-rA, Japan) using a diffractometer with Cu Kα radiation, λ = 1.54184 Å in the range of 2θ = 20–70°, scan rate of 4° min^{-1}. Thermogravimetric analysis (TGA) was performed on a Shimadzu DTG-50 thermal analyzer under 25–900 °C at a rate of 10 °C min^{-1}, and dried air used as the carrier gas with a flow rate of 40 mL min^{-1}. The ultraviolet–visible diffuse reflectance spectra (UV–vis DRS) was measured for photochemical properties using a TU-1901 in combination with a single reflection internal accessory (Beijing Purkinje General Instrument Co., Ltd.). The electrochemical properties were measured by CHI660D potentiostat (Shanghai Chen hua Instrument Co., Ltd.) in 0.1 mol L^{-1} $KHCO_3$ with sweep rate of 50 mV s^{-1}. The as-prepared electrode worked as working electrode, platinum wire as counter electrode, and Hg/Hg_2Cl_2 in saturated KCl solution as reference electrode, respectively.

The reduction of CO_2 was measured at different potentials in 0.1 mol L^{-1} $KHCO_3$ solution with CO_2 purged continuously. The products were immediately detected and analyzed by gas chromatography (GC-9A, Shimadzu). The GC was equipped with glass packed column (2 m, inner diameter 3 mm, Parapok Q, 80–100) and flame ionization detector. The column was kept at 100 °C and the detector was at 150 °C. High purity N_2 worked as carrier gas with a flow rate of 30 sccm. The standard of potential in the figures is against the SCE.

3. Results and discussion

Fig. 1a is the top view of the Fe_2O_3 NTs, it shows that the as-prepared Fe_2O_3 NTs are distributed orderly like volcanoes and each volcano contained many nanotubes. The insert map demonstrates that the nanotube structure with pore diameter of 25–30 nm. The sectional view of Fe_2O_3 NTs (Fig. 1b) indicated perthitic texture, it further demonstrates that Fe_2O_3 NTs nanowall presents nanotube structure with thickness of 8–10 nm, the TEM image (Fig. 1e) can further prove that. From Fig. 1c and d, CoPc shows as ribbon structure with length of 7.1 μm, width of 700 nm, and ribbons were distributed evenly on the surface of Fe_2O_3 NTs and no aggregation, and it grew in one-dimensional ribbon formation.

Fig. 2a is the DTA and TG curves of the CoPc. The DTA curve coincided with TG curve almostly. The weightlessness peak is located at 494.6 °C, and the primary reason is the thermolysis of the CoPc, which is consistent with the literature reported [2]. It further demonstrates that the ribbon material assembled on the Fe_2O_3 NTs surface actually is CoPc.

The FT-IR absorption spectra of in situ CoPc are shown in Fig. 2b. It can be seen from Fig. 2b that the bands 731 cm^{-1} is assigned to the vibration of Pc ring, the 1523 cm^{-1} and 1610 cm^{-1} bands are the vibrations of C=N and pyrrole ring, the 1720 cm^{-1} band is the C=C stretching, the 1425 cm^{-1} and 1470 cm^{-1} are the stretching of C—C and C—N, the 913 cm^{-1} band is assigned to the metal–ligand Co—N vibration. It proves that metal has coordinated with nitrogen of Pc ring and CoPc is successfully synthesized.

Fig. 3 shows the XRD patterns of CoPc-Rs/Fe_2O_3 NTs and Fe_2O_3 NTs. The strong and sharp diffraction peaks indicates good crystallizations [25]. The 24.19°, 33.31°, 35.61°, 40.82°, 43.21°, 49.64°, 54.25° and 62.64° correspond with the (0 1 2), (1 0 4), (1 1 0), (1 1 3), (2 0 2), (0 2 4), (1 1 6) and (2 1 4) crystal faces of Fe_2O_3 NTs, respectively. Lattice parameters of a = 4.7528 Å, c = 3.1639 Å is consistent with the JCPDS card No. 33-0664 [26]. After assembling CoPc on Fe_2O_3 NTs, the new appearance peaks of 7.11° and 9.43° correspond with the (0 0 1) and (1 0 0) crystal faces of CoPc [2]. In addition, the characteristic peak of Fe_2O_3 NTs is almost immovable, it demonstrates that the CoPc not covers on the surface of Fe_2O_3 NTs completely, which is consistent with the SEM image of Fig. 1c.

Fig. 4a shows the UV–vis patterns of the CoPc-Rs/Fe_2O_3 NTs and the Fe_2O_3 NTs. From the figure, it can be seen clearly that the absorption intensity of the Fe_2O_3 NTs is enhanced obviously after assembling CoPc, and the visible light absorption peak of the Fe_2O_3 NTs varies from 500 nm to 550 nm after assembling CoPc, which demonstrates that the visible light absorption region of the Fe_2O_3 NTs is broadened by CoPc, because it occurred interaction after assembling CoPc on Fe_2O_3 NTs. The center metal ions of the CoPc engenders low-binding with the O of the Fe_2O_3 NTs in the axis direction, which makes the electron density of the Pc ring enhanced, so the loss of electrons on CoPc occurs easily after being excited,

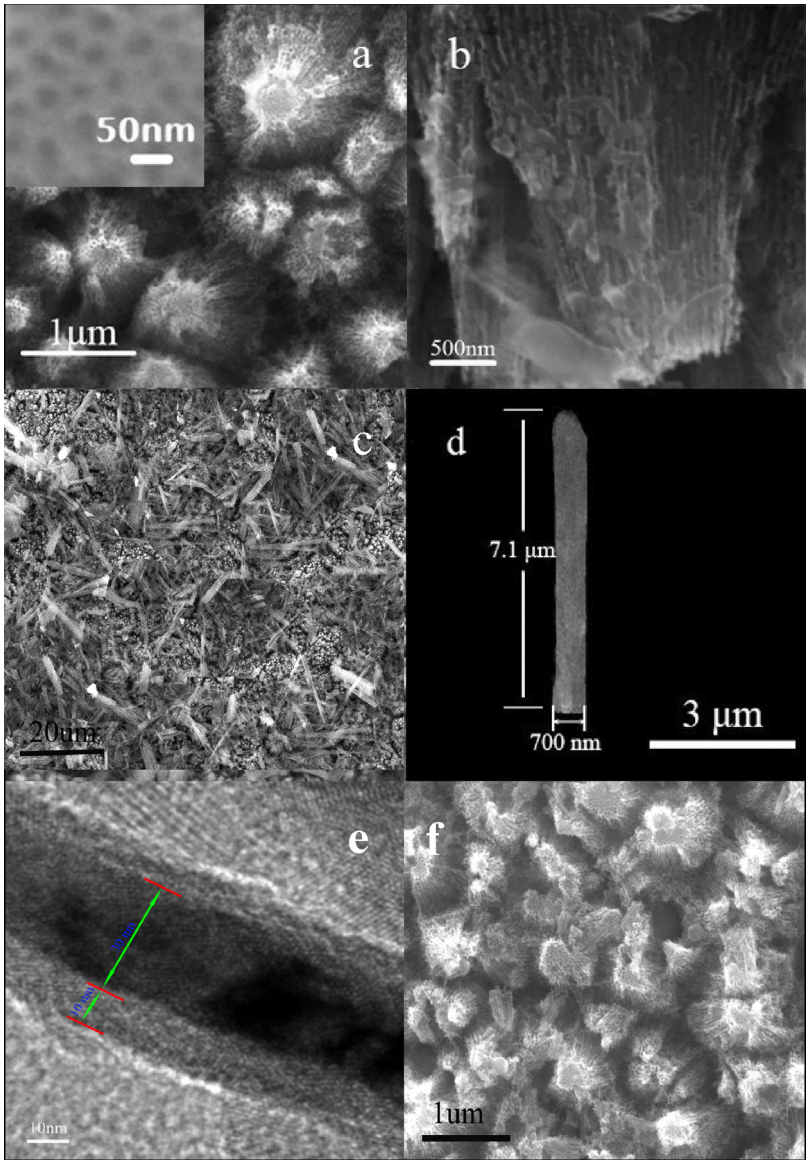

Fig. 1. (a) SEM image of Fe_2O_3 NTs (inset: high-magnification SEM image); (b) cross-sectional view of Fe_2O_3 NTs; (c) SEM image of CoPc-Rs/Fe_2O_3 NTs; (d) SEM image of CoPc-Rs; (e) TEM image of Fe_2O_3 NTs; and (f) SEM image of CoPc-Rs/Fe_2O_3 NTs after using.

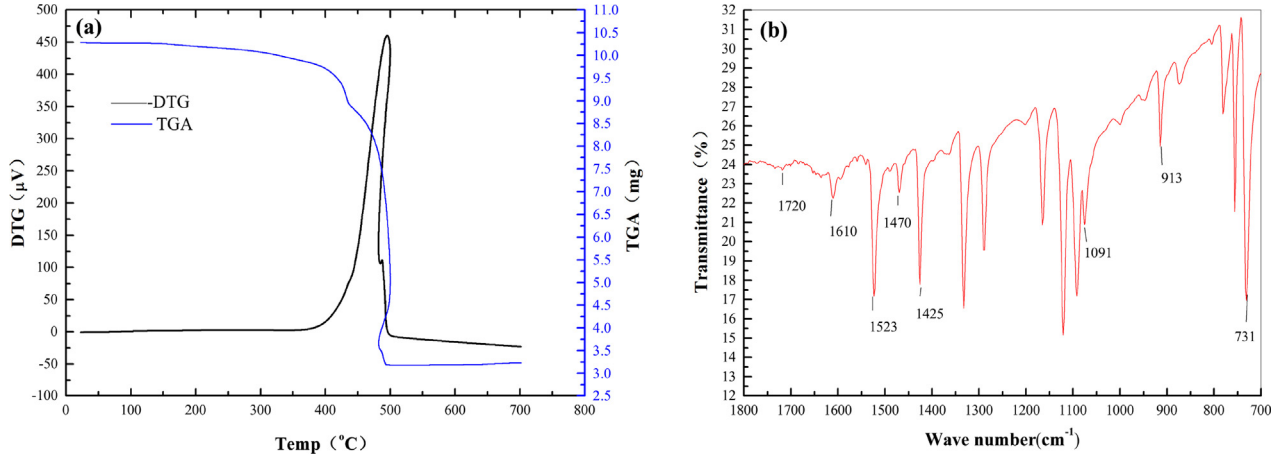

Fig. 2. (a) DGA-TG image of CoPc and (b) FT-IR pattern of CoPc.

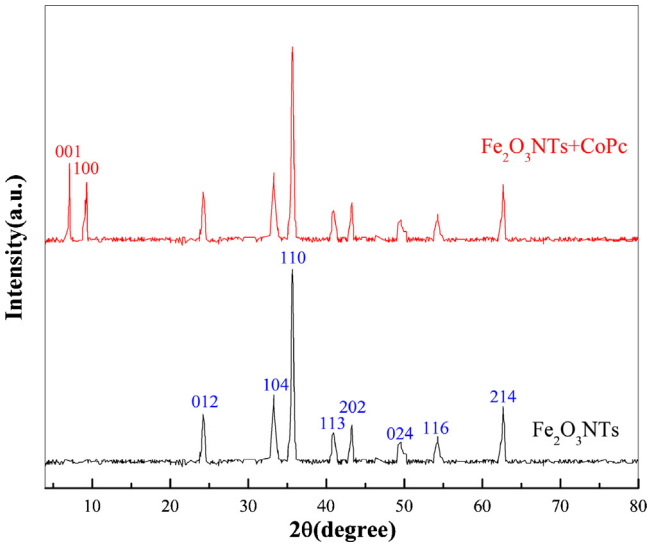

Fig. 3. XRD patterns of CoPc-Rs/Fe_2O_3 NTs and Fe_2O_3NTs.

and then occur the red shift phenomenon mentioned above. The peaks of 625 nm and the 693 nm are the characteristic absorption peak of CoPc monomer from Fig. 4a, it illustrates that there is no aggregation among CoPc after assembling onto the Fe_2O_3 NTs [27]. The energy gaps of Fe_2O_3 NTs and CoPc-Rs/Fe_2O_3 NTs are 2.02 eV and 1.72 eV which narrows 0.30 eV comparing to Fe_2O_3 NTs. So the CoPc-Rs/Fe_2O_3 NTs becomes more easily excited by visible light after the CoPc being assembled.

The Fe_2O_3 NTs and the CoPc-Rs/Fe_2O_3 NTs PC reduction ability for CO_2 are studied by *i–t* curve under open circuit potential. There are two main factors that could increase the current density, one is the hydrogen evolution reaction (HER), and the other is the reduction of CO_2. Fig. 5a shows the photo-current and dark-current transients on Fe_2O_3 NTs in 0.1 mol L^{-1} $KHCO_3$ saturated with N_2 or CO_2. It can be seen that the current density of Fe_2O_3 NTs in CO_2 atmosphere is about 1.7 times that of in N_2 atmosphere, which explains that the Fe_2O_3 NTs has certain reduction ability for CO_2. Meantime, it can be found that the light response of Fe_2O_3 NTs is inconspicuous between with light and without light, and the current density decreases with time increasing, it can be explained that the PC ability of Fe_2O_3 NTs is limited. It can be seen that the nanotubes did not peel off from the Fe substrate, but it appeared a certain degree of corrosion from Fig. 1f, this can further prove the current density decrease. Fig. 5b shows the photo-current and dark-current transients on CoPc-Rs/Fe_2O_3 NTs with N_2 or CO_2. It can be seen that the current density of CoPc-Rs/Fe_2O_3 NTs is about 1.6 times that of Fe_2O_3 NTs in CO_2 atmosphere, which can be demonstrated that CoPc enhances the PC reduction ability of Fe_2O_3 NTs. The current density difference value of CoPc-Rs/Fe_2O_3 NTs with light and dark is 0.45 mA cm^{-2} saturated with CO_2, and the difference value is 0.03 mA cm^{-2} saturated with N_2. The former is 15 times of the latter, it demonstrates that the introduction of CoPc-Rs significantly increased the PC reduction ability of CO_2 under visible light irradiation. It was attributed to the one-dimensional special structure and characteristic of CoPc, the outstanding photosensitiveness could enhance the absorption capacity of visible light, and the excellent electron transfer capability can separate light-generated electron and hole effectively, which further improved the PC performance.

The linear sweep voltammetry (LSV) is conducted in 0.1 mol L^{-1} $KHCO_3$ solution with a standard three-electrode configuration. Fig. 6a and b shows that the current density changes with the potential. There are two main factors that influence the current density, one is the redox of H_2O, and the other is the PEC

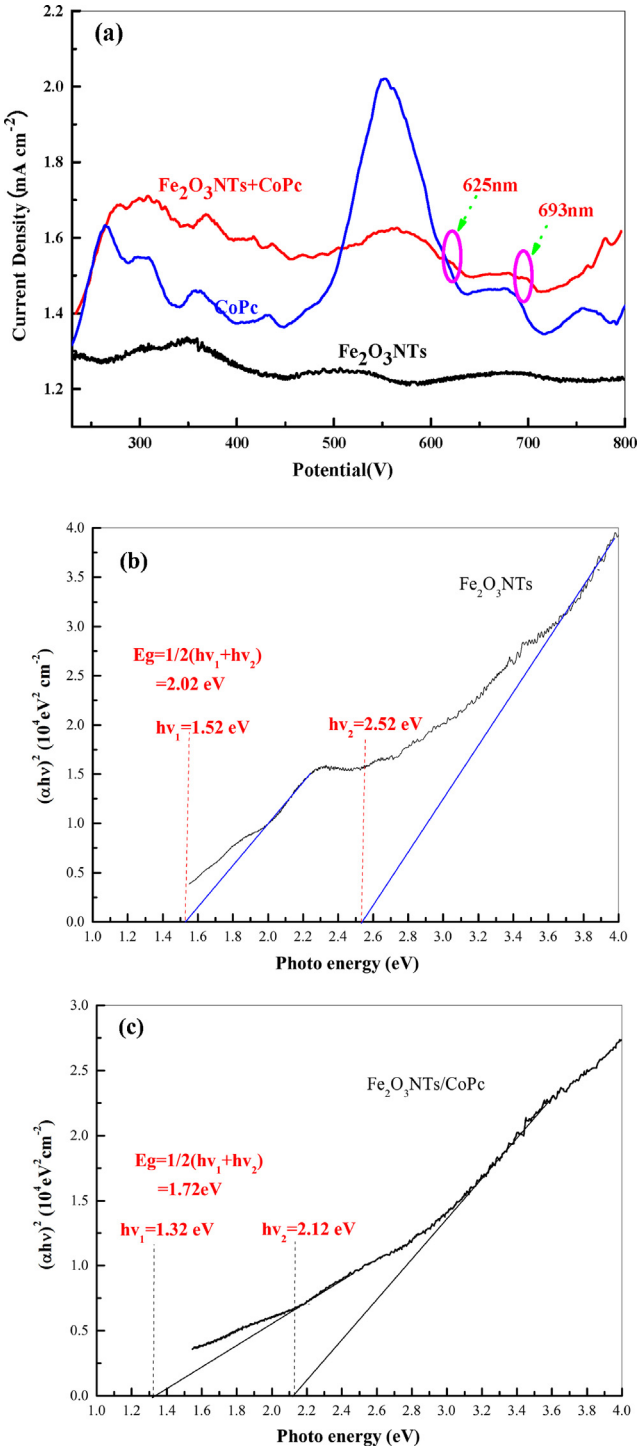

Fig. 4. (a) The UV–vis DRS spectrums of CoPc-Rs/Fe_2O_3 NTs, CoPc and Fe_2O_3 NTs; (b) plot analysis of optical band gap of Fe_2O_3 NTs; and (c) plot analysis of optical band gap of CoPc-Rs/Fe_2O_3 NTs.

reduction of CO_2 to organic compounds. It can be seen obviously that Fe_2O_3 NTs and CoPc-Rs/Fe_2O_3 NTs show the same rule that the current density with CO_2 is greater than with N_2. It illustrates that the two electrodes have certain catalytic reduction ability for CO_2. Without light, the net current density ($i_{CO2} - i_{N2}$) of CoPc-Rs/Fe_2O_3 NTs and Fe_2O_3 NTs is 0.85 mA cm^{-2} and 0.04 mA cm^{-2} at −1.3 V, it indicates that CoPc-Rs/Fe_2O_3 NTs has better EC reduction ability for CO_2. And it can be seen that the starting potential of EC reduction on Fe_2O_3 NTs is −1.28 V and CoPc-Rs/Fe_2O_3 NTs is

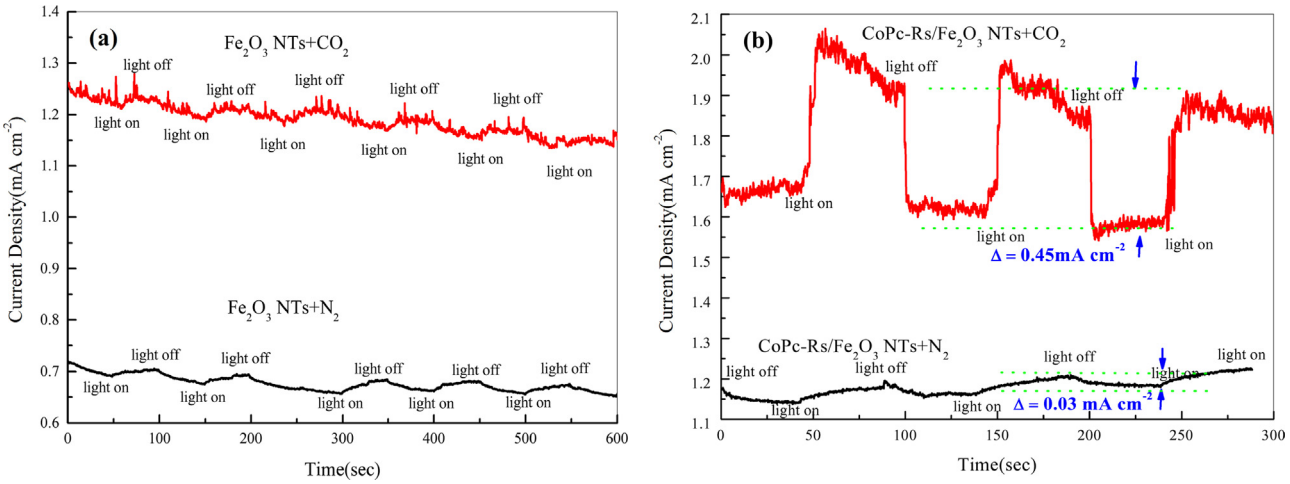

Fig. 5. *i–t* curves of (a) Fe_2O_3 NTs and (b) CoPc-Rs/Fe_2O_3 NTs under open circuit potential.

−1.24 V. The latter shifts forward 40 mV compared to the former. It demonstrates that the assembling of CoPc decreases the overpotential of EC reduction CO_2, which in favor of the EC reduction CO_2. Furthermore, the electrochemical impedance spectroscopy (EIS) of CoPc-Rs/Fe_2O_3 NTs (600 Ω) reduces 900 Ω than that of Fe_2O_3 NTs (1500 Ω). The reduced impedance confirms that the composite has better electron transfer capacity, which results in the excellent EC performance [28].

When light was further added, it can be seen that the net current density ($i_{CO2} - i_{N2}$) of PEC reduction of CO_2 on CoPc-Rs/Fe_2O_3 NTs and Fe_2O_3 NTs was 1.30 mA cm^{-2} and 0.17 mA cm^{-2}, respectively. The former is 7.65 times of the latter. It illustrated that

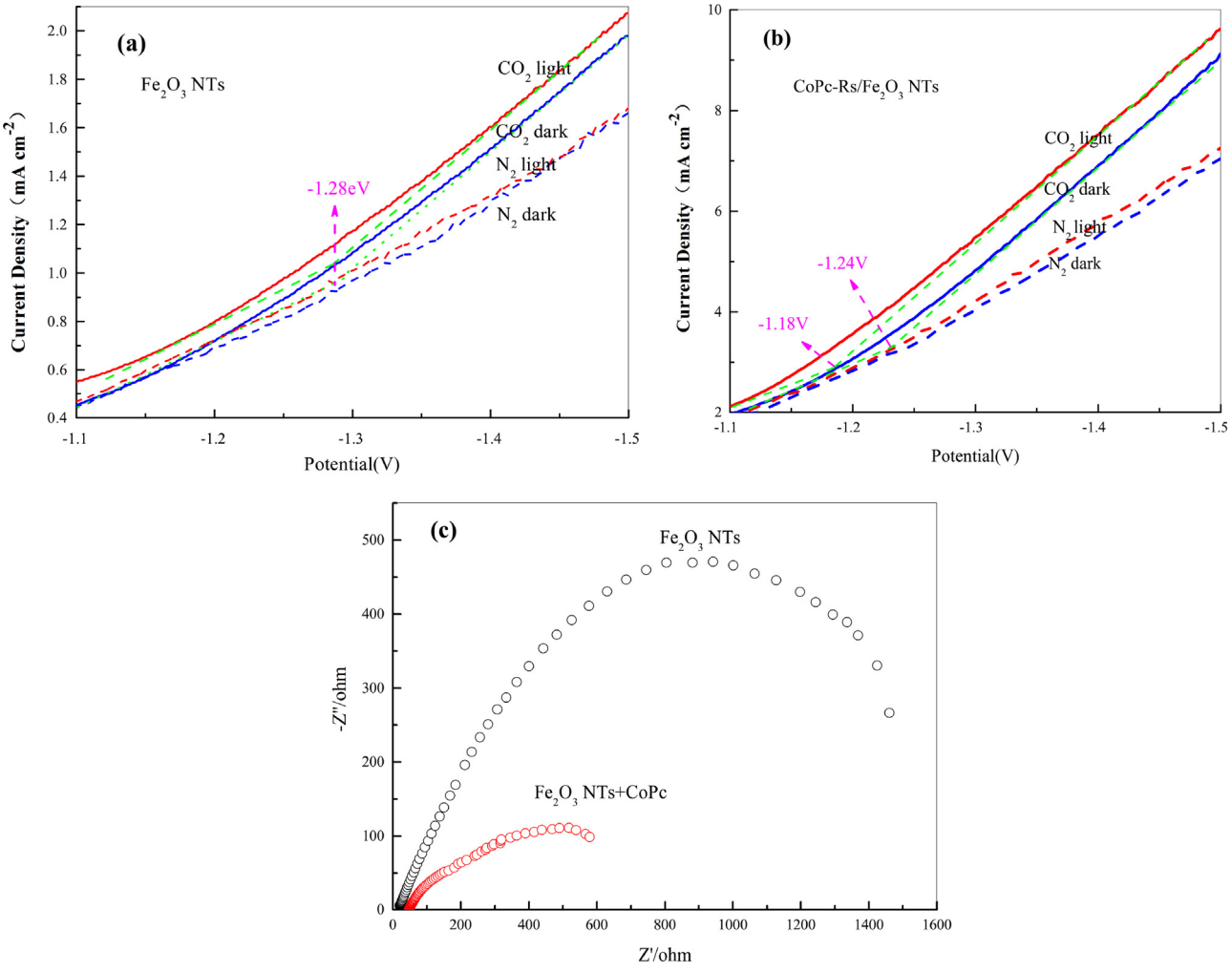

Fig. 6. (a) LSV curves of Fe_2O_3 NTs; (b) LSV curves of CoPc-Rs/Fe_2O_3 NTs; and (c) EIS of Fe_2O_3 NTs and CoPc-Rs/Fe_2O_3 NTs under illumination.

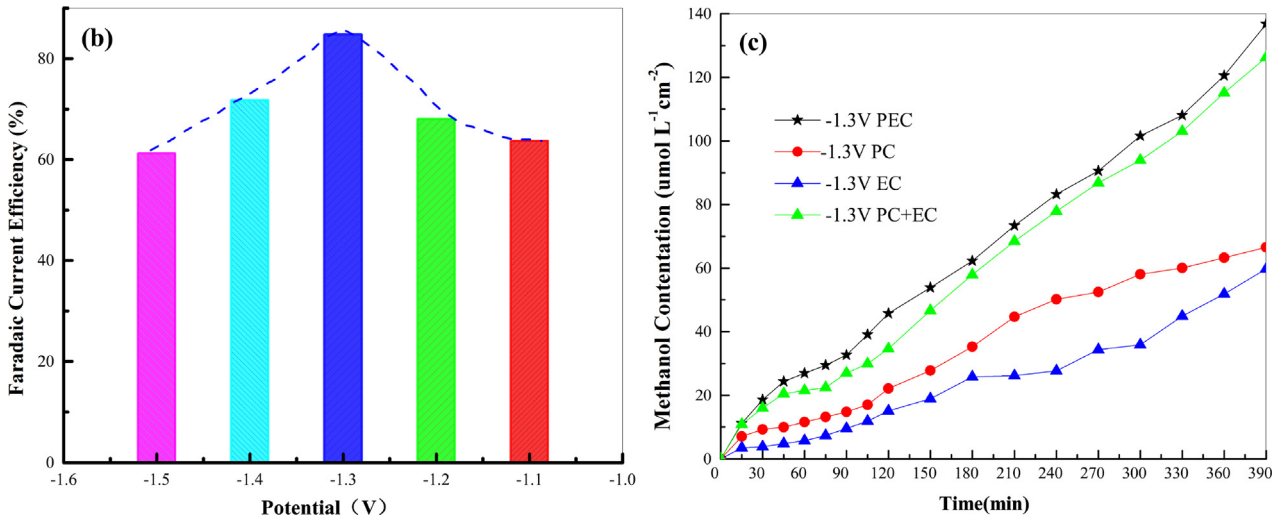

Fig. 7. (a) Methanol concentration of CoPc-Rs/Fe_2O_3 NTs of PEC reduction CO_2 under different potentials; (b) faradaic current efficiency of CoPc-Rs/Fe_2O_3 NTs of PEC CO_2 reduction with different potentials; and (c) methanol concentration of CoPc-Rs/Fe_2O_3 NTs of PEC, PC and EC CO_2 reduction at −1.3 V.

CoPc-Rs/Fe_2O_3 NTs has excellent PC reduction and EC reduction ability simultaneously, and has more excellent in situ PEC reduction ability. With the further application of light, it was found that the PEC reduction starting potential on Fe_2O_3 NTs for CO_2 was still −1.28 V, but the PEC reduction starting potential on CoPc-Rs/Fe_2O_3 NTs has been advanced to −1.18 V, which shifted positively compared with EC. It illustrated that the light further decreased the overpotential of CO_2 reduction, and had good synergistic effect with EC reduction, which could promote the catalytic reduction of CO_2 further.

The CO_2 reduction experiments were performed in a quartz cell with circulating cooling water. The predominant reaction product analyzed by GC is methanol. The PEC activity of CoPc-Rs/Fe_2O_3 NTs is evaluated further according to methanol production. The methanol yield of CoPc-Rs/Fe_2O_3 NTs increases with continuous visible light irradiation under different applied potential (vs. SCE) shown in Fig. 7a. From −1.1 V to −1.5 V, the methanol output increases firstly, reaches a peak at −1.3 V and then decreases, the largest methanol yield is 138 μmol L^{-1} cm^{-2} when the reaction time reaches 390 min. The maximum methanol output under −1.3 V could be explained as follows: the faradaic current efficiency increases with the negatively shifted applied potential, it reaches peak (84.6%) at −1.3 V, when the applied potential is more negative than −1.3 V, HER takes place, the reactions of CO_2 reduction and HER are competitive reactions on the surface of the electrode, which results in the decrease of the faradaic current efficiency (Fig. 7b). At the same time, the predominant product methanol of the CO_2 reduction in the PC, EC, PC + EC and PEC process was also analyzed (Fig. 7c). It illustrates that the methanol output of the PEC reduction process is bigger than that of the simple addition of PC reduction and EC reduction. After 390 min, the methanol concentration of PEC, PC + EC, PC and EC reduction are 138 μmol L^{-1} cm^{-2}, 126 μmol L^{-1} cm^{-2}, 66 μmol L^{-1} cm^{-2} and 60 μmol L^{-1} cm^{-2}, respectively. In conclusion, when the electric and light was simultaneously added in situ, it generated the 1 + 1 > 2 synergistic effect between the PC reduction and the EC reduction on the CoPc-Rs/Fe_2O_3.

Based on the experimental results and literature reports, the mechanism for the PEC reduction of CO_2 to methanol was deduced (Fig. 8). The reduction of CO_2 to methanol is six electrons reaction. Firstly, what is the special explanation is where the electron and hydrogen proton come from. For the electrons, it is deduced from two aspects. One is generated from the light excited. The conduction band of CoPc-Rs/Fe_2O_3 NTs is located at −0.73 eV which is more negative than the reduction potential of CO_2/CH_3OH (−0.38 eV). The light-generated electrons have enough reduction ability to transform CO_2 to methanol [29]. The other is generated from applied external potential, which can supply enough electrons for the CO_2 EC reduction at the cathode position. For the protons, it is also deduced from two aspects. One hand, the valance band of CoPc-Rs/Fe_2O_3 NTs is located at 1.05 eV, which is more positive than the oxidation potential of H_2O/O_2 (0.82 V). So the illuminated CoPc-Rs/Fe_2O_3 NTs has sufficient oxidation ability to split H_2O and get O_2 and hydrogen proton [30]. It is one reason that light can enhance the CO_2 EC reduction ability greatly. On the other hand, the protons come from the applied external potential. When the potential was positive enough, the anode can also split H_2O to get hydrogen proton.

Secondly, the process of CO_2 PEC reduction has been concretely deduced. As a light-sensitive material, the CoPc is excited from ground state (P) to singlet state (P^*) firstly. The photoelectrons from P–P^* transition caused by light generated and the electrons offered by applied external potential at the cathode participate the CO_2 reduction process jointly. CO_2 is firstly reduced to CO_2^- radical by electron, and then the CO_2^- radical are easily combined with the Co cation in CoPc to form Co—O, and then produces the production P_1.

Then the [CoPc(CO_2)] anion (P_1) with negative charge recombines with the dissociative hydrogen proton on the electrode surface, and then gets the production P_2, but the formed structure is unstable and vulnerable by electron, and further forming Co—O to obtain the production P_3. Then P_3 combines with the hydrogen proton to form the CoPc-CO_2H_2 (coordination compound P_4). The P_4 is vulnerable by electron to lead the breakage of C—O, and combines with hydrogen proton to obtain the production P_5 and P_6. Finally, the Co—O separates and combines with hydrogen proton to receive the CoPc, H_2O and CH_3OH. After the PEC reduction of CO_2, CoPc is scraped from the surface of electrode, it was found that there are still two strong absorption peaks at 627 nm and 693 nm generated from the electron transition of $a_{1u}(\pi) - e_g(\pi^*)$ of Q band of CoPc. It is the same as literature reported of the absorption value of monomer CoPc [27]. It confirmed that the CoPc did not engender dimerization, and further indicated the CoPc has reborn after the PEC reduction process and could repeated recycling, which supported the deduced mechanism.

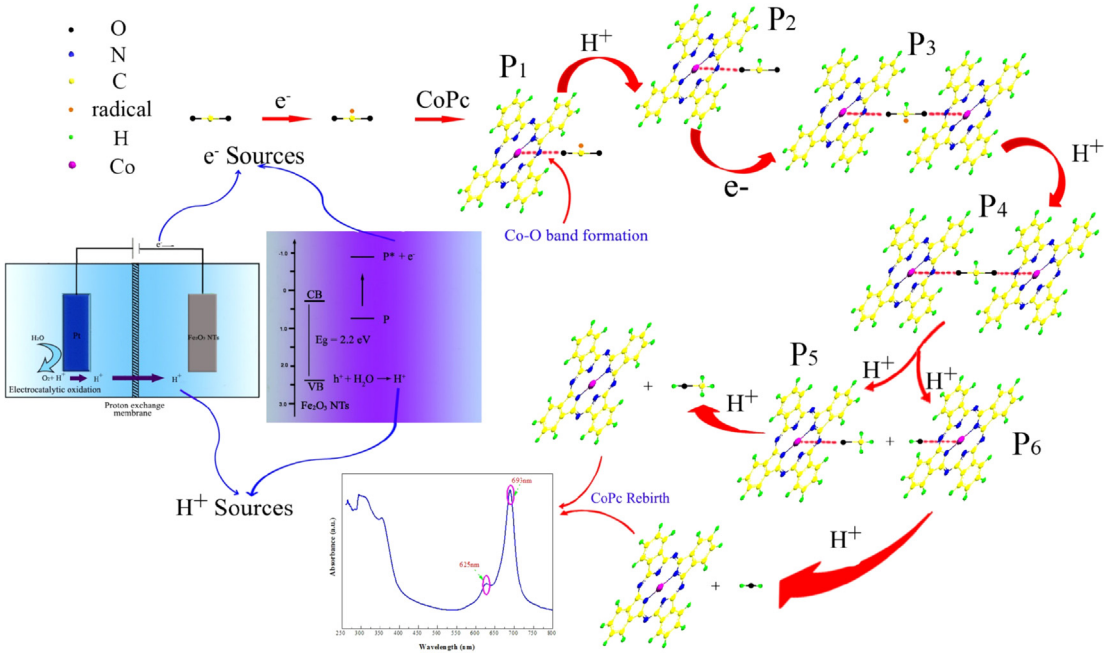

Fig. 8. The mechanism of PEC reduction of CO_2 on CoPc-Rs/Fe_2O_3 NTs.

4. Conclusion

The anodic oxidation was used to in situ prepare volcano Fe_2O_3 NTs. One-dimensional CoPc-Rs in situ assembling onto Fe_2O_3 NTs obtained the CoPc-Rs/Fe_2O_3 NTs. It showed that the CoPc-Rs with length of 7.1 μm and width of 700 nm distributed evenly on the Fe_2O_3 NTs surface and it grew along (0 0 1) crystal face. After assembling CoPc-Rs on Fe_2O_3 NTs, on the one hand, the PC performance was improvement due to the enhancement of absorbing visible light and the narrowed energy band gap. On the other hand, EC ability was improved by decreasing the resistance (900 Ω), improving electron transfer ability, and decreasing the overpotential (40 mV) of CO_2 reduction. In the PEC reduction process at −1.3 V, the net current density ($i_{CO2} - i_{N2}$) of CoPc-Rs/Fe_2O_3 NTs was 7.65 times that of the Fe_2O_3 NTs. The overpotential of CoPc-Rs/Fe_2O_3 NTs PEC reduction for CO_2 brought forward 100 mV than that of Fe_2O_3 NTs, which exhibits outstanding PEC reduction performance on CoPc-Rs/Fe_2O_3 NTs. The methanol concentration of PEC reduction CO_2 (138 μmol L^{-1} cm^{-2}) was bigger than that of the simple addition (126 μmol L^{-1} cm^{-2}) of the PC and EC after 390 min, which embodied the excellent synergic effect between the PC reduction and EC reduction. The faradaic current efficiency reached up to 84.6% at this moment. Meantime, the electron and hydrogen proton sources of the PEC reduction CO_2 have been deduced and the mechanism of transforming CO_2 to CH_3OH has been also reasonably deducted. This paper offered a new method for designing the catalyst for PEC synergistic reduction of CO_2, it also had positive significance for reducing carbon emission and cycling carbonaceous energy.

Acknowledgements

This research was supported by the National Natural Science Foundation of China (Grant No. 21203114), Key Projects in the National Science & Technology Pillar Program during the Twelfth Five-year Plan Period (Grant No. 2011BAD11B01), and Promotive Research Fund for Excellent Young and Middle-aged Scientists of Shandong Province (Grant No. BS2012NJ008), and Science and Technology Development Planning of Shandong Province (Grant No. 2013GCX20109). We are grateful to the foundation supported by Shandong Jingbo Holdings Corporation.

References

[1] M. Cokoja, C. Bruckmeier, B. Rieger, W.A. Herrmann, F.E. Kühn, Angewandte Chemie International Edition 50 (2011) 8510–8537.
[2] Z. Zhao, J. Fan, M. Xie, Z. Wang, Journal of Cleaner Production 17 (2009) 1025–1029.
[3] S. Navalón, A. Dhakshinamoorthy, M. Álvaro, H. Garcia, ChemSusChem 6 (2013) 562–577.
[4] E.E. Benson, C.P. Kubiak, A.J. Sathrum, J.M. Smieja, Chemical Society Reviews 38 (2009) 89–99.
[5] M. Le, M. Ren, Z. Zhang, P.T. Sprunger, R.L. Kurtz, J.C. Flake, Journal of the Electrochemical Society 158 (2011) E45–E49.
[6] G. Centi, S. Perathoner, G. Winè, M. Gangeri, Green Chemistry 9 (2007) 671–678.
[7] M. North, R. Pasquale, C. Young, Green Chemistry 12 (2010) 1514–1539.
[8] M.E. Berndt, D.E. Allen, W.E. Seyfried, Geology 24 (1996) 351–354.
[9] X. Guo, D. Mao, S. Wang, G. Wu, G. Lu, Catalysis Communications 10 (2009) 1661–1664.
[10] A.J. Morris, R.T. McGibbon, A.B. Bocarsly, ChemSusChem 4 (2011) 191–196.
[11] B. Kumar, M. Llorente, J. Froehlich, T. Dang, A. Sathrum, C.P. Kubiak, Annual Review of Physical Chemistry 63 (2012) 541–569.
[12] Q. Liu, Y. Zhou, J. Kou, X. Chen, Z. Tian, J. Gao, S. Yan, Z. Zou, Journal of the American Chemical Society 132 (2010) 14385–14387.
[13] N.S. Spinner, J.A. Vega, W.E. Mustain, Catalysis Science & Technology 2 (2012) 19–28.
[14] P. Li, H. Hu, J. Xu, H. Jing, H. Peng, J. Lu, C. Wu, S. Ai, Applied Catalysis B: Environmental 147 (2014) 912–919.
[15] P. Li, H. Wang, J. Xu, H. Jing, J. Zhang, H. Han, F. Lu, Nanoscale 5 (2013) 11748–11754.
[16] Q. Huang, F. Kang, H. Liu, Q. Li, X. Xiao, Journal of Materials Chemistry A 1 (2013) 2418–2425.
[17] Y. Wang, Y.-n. Zhang, G. Zhao, H. Tian, H. Shi, T. Zhou, ACS Applied Materials & Interfaces 4 (2012) 3965–3972.
[18] H. Gao, W. Chen, J. Yuan, Z. Jiang, G. Hu, W. Shangguan, Y. Sun, J. Su, RSC Advances 3 (2013) 8559–8564.
[19] A.J. Cowan, C.J. Barnett, S.R. Pendlebury, M. Barroso, K. Sivula, M. Grätzel, J.R. Durrant, D.R. Klug, Journal of the American Chemical Society 133 (2011) 10134–10140.
[20] A. Mao, K. Shin, J.K. Kim, D.H. Wang, G.Y. Han, J.H. Park, ACS Applied Materials & Interfaces 3 (2011) 1852–1858.
[21] G. Zhang, Y. Gao, Y. Zhang, Y. Guo, Environmental Science & Technology 44 (2010) 6384–6389.
[22] X. Zhu, Y. Zhu, S. Murali, M.D. Stoller, R.S. Ruoff, ACS Nano 5 (2011) 3333–3338.
[23] D.K. Zhong, D.R. Gamelin, Journal of the American Chemical Society 132 (2010) 4202–4207.
[24] K. Sakamoto, E. Ohno-Okumura, Materials 2 (2009) 1127–1179.

[25] Z. Zhang, M.F. Hossain, T. Takahashi, Applied Catalysis B: Environmental 95 (2010) 423–429.
[26] Z. Sun, H. Yuan, Z. Liu, B. Han, X. Zhang, Advanced Materials 17 (2005) 2993–2997.
[27] J. Han, X. Xu, X. Rao, M. Wei, D.G. Evans, X. Duan, Journal of Materials Chemistry 21 (2011) 2126–2130.
[28] S. Wang, X. Jiang, H. Zheng, H. Wu, S.-J. Kim, C. Feng, Nanoscience and Nanotechnology Letters 4 (2012) 378–383.
[29] J. Mao, T. Peng, X. Zhang, K. Li, L. Ye, L. Zan, Catalysis Science & Technology 2 (2013) 1253–1260.
[30] J. Yuan, C. Hao, Solar Energy Materials and Solar Cells 108 (2013) 170–174.